Supporting Information for
Competing Weak Localization and Weak Antilocalization in Ultrathin Topological Insulators

Murong Lang,[†,ll] *Liang He,*[†,ll, *] *Xufeng Kou,*[†,ll] *Pramey Upadhyaya,*[†] *Yabin Fan,*[†] *Hao Chu,*[⊥] *Ying Jiang,*[§] *Jens H. Bardarson,*[‡, #] *Wanjun Jiang,*[†] *Eun Sang Choi,*[£] *Yong Wang,*[§] *Nai-Chang Yeh,*[⊥] *Joel Moore,*[‡,#] *and Kang L. Wang*[†,*]

[†] Department of Electrical Engineering, University of California, Los Angeles, California 90095

[‡] Department of Physics, University of California, Berkeley, CA 94720

[#] Materials Sciences Division, Lawrence Berkeley National Laboratory, Berkeley, CA 94720

[§] Center of Electron Microscopy, State Key Laboratory of Silicon Materials, Department of Materials Science and Engineering, Zhejiang University, Hangzhou, 310027, China

[⊥] Department of Physics, California Institute of Technology, Pasadena, CA 91125

[£] National High Magnetic Field Laboratory, Tallahassee, FL 32310

[ll] These authors contribute equally to this work

[*]To whom correspondence should be addressed. E-mail: wang@ee.ucla.edu, heliang@ee.ucla.edu

1. MBE Growth of $(Bi_{0.57}Sb_{0.43})_2Te_3$.

High-quality single crystalline $(Bi_{0.57}Sb_{0.43})_2Te_3$ thin films were conducted in a PerkinElmer MBE system under an ultra-high vacuum environment; MBE is proven to be a powerful and reliable technique to produce ultrathin TI films with accurate thickness control to a few quintuple layers.[1-3] Intrinsic GaAs (111) wafers ($\rho > 10^6\ \Omega\cdot$cm) were cleaned by a standard Radio Corporation of America (RCA) procedure before being transferred into the growth chamber. Then GaAs substrates were annealed in the chamber under Se-protective environment at ~580 ˚C to remove the native oxide on the surface. After removing the native oxides, the GaAs substrate has shown clear 2D pattern with a bright specular spot (Figure S1**a**), indicating the epi-ready surface for subsequent growth. During growth, Bi, Sb and Te cells were kept at 470, 395 and 320°C respectively, while GaAs (111) substrate was set at 200°C (growth temperature). Figure S1**b** shows a large-scale atomic force microscope (AFM) image of an as-grown $(Bi_{0.57}Sb_{0.43})_2Te_3$ film with a thickness of 9 QL, exhibiting terraces over 500 nm in size. The surface consists of triangle-shaped terraces and steps, indicative of a hexagonal crystal structure inside (0001) planes.

In-situ growth dynamics are monitored by reflection high energy electron diffraction (RHEED) measurements. Digital images of the RHEED were captured using a KSA400 system made by K-space Associate, Inc. Growth rate can be estimated as 1 QL/min from the periodic RHEED oscillations which started from the first layer of the growth (Figure S1**c**).D-spacing of surface lattice change during growth after 1st $(Bi_{0.57}Sb_{0.43})_2Te_3$ layer growth as indicated in Figure S1**d**. 2 nm Aluminum (Al) was subsequently deposited *in-situ* at 20 ˚C to protect the epi-layer from unintentional doping induced by ambient environment.[4] Al film was later naturally oxidized to form Al_2O_3 after the sample was taken out of the chamber and exposed in air, which also further serves as a good seeding layer of the high-k dielectric oxide stack grown by the atomic layer deposition (ALD) process.

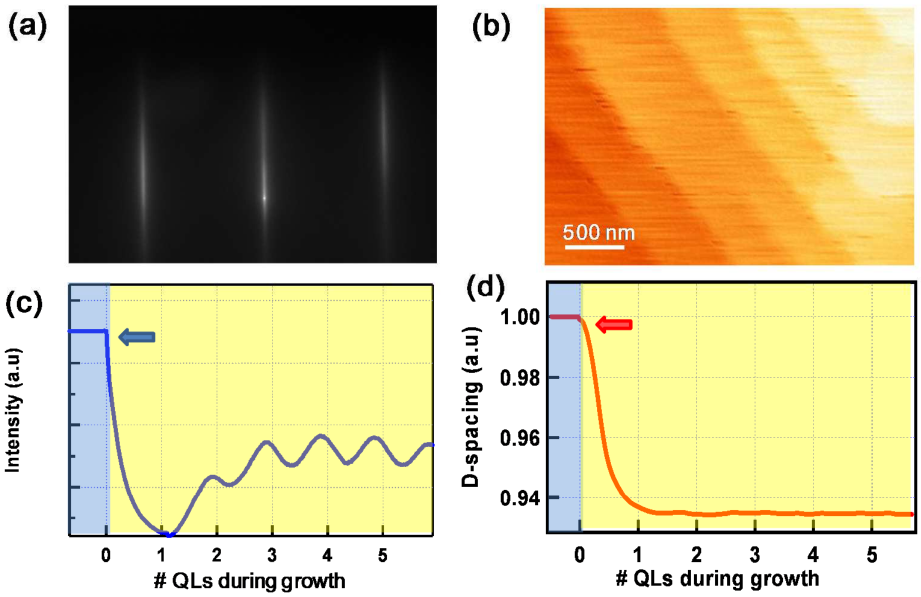

Figure S1. $(Bi_{0.57}Sb_{0.43})_2Te_3$ compound growth characterization. a, RHEED pattern along $[11\bar{2}0]$ direction of an as-grown surface of $(Bi_{0.57}Sb_{0.43})_2Te_3$ with a thickness of 9 QLs. **b**, An AFM image of the TI thin film with terrace size exceeding 500 nm. **c**, RHEED oscillations of intensity of the specular beam. The oscillation period is found to be 60 s, corresponding to a growth rate of ~ 1 QL/min. **d**, D-spacing of surface lattice change during growth. The arrow indicates that the surface morphology has converted from GaAs to after 1st $(Bi_{0.57}Sb_{0.43})_2Te_3$ layer growth.

2. Sample Characterization Methods.

(1) **TEM**. High-resolution TEM experiments were performed on a FEI TITAN Cs-corrected high-resolution STEM operating at 200 KV. The HAADF (high angle annular dark field) images were acquired by a Fischione HAADF detector. (2) **EDX**. EDX was performed with a FEI Tecnai G2 F20 S-Twin TEM. (3) **Transport measurements**. High magnetic field and low temperature measurements were conducted at National High Magnetic Field Laboratory with the application of DC magnetic field up to ± 18 T. The temperature range is from 0.3 to 60 K. Standard four-probe measurements were carried out with an ac current sourced from a Keithley 6221. Multiple lock-in-amplifiers were used to measure the longitudinal and transverse resistance. (4) **STS measurements**. The sample with

2 nm passivated Al_2O_3 was first etched in 5% HF solution for 10 seconds and immediatly transferred to the cryogenic probe of a homemade STM sample holder in argon environment. The STM is then pumped down to 8×10^{-5} Torr vacuum and then cooled down to 77K. The spectroscopy data was acquired over a 64×64 grid on an area of 10 nm×10 nm

3. Device Fabrication.

The MBE-grown $(Bi_{0.57}Sb_{0.43})_2Te_3$ thin film was first patterned into a micron-scale Hall bar geometry using conventional optical photolithography and a subsequent CHF_3 dry-etching of 15 s. Hall bar contacts were defined by photolithography and followed by *e*-beam evaporation of 10 nm chromium (Cr) and 100 nm gold (Au). A 25 nm-thick Al_2O_3 dielectric layer was conformally deposited by ALD at 250°C to serve as the high-k gate dielectric. Another step of photolithography was needed to open window, and dry etching was carried out to etch the Al_2O_3 in the contact area with subsequent dip in 5% diluted HF. Finally, the top-gate electrode and Hall channel contacts were defined and followed by metal deposition of Cr/Au (10 nm/100 nm).

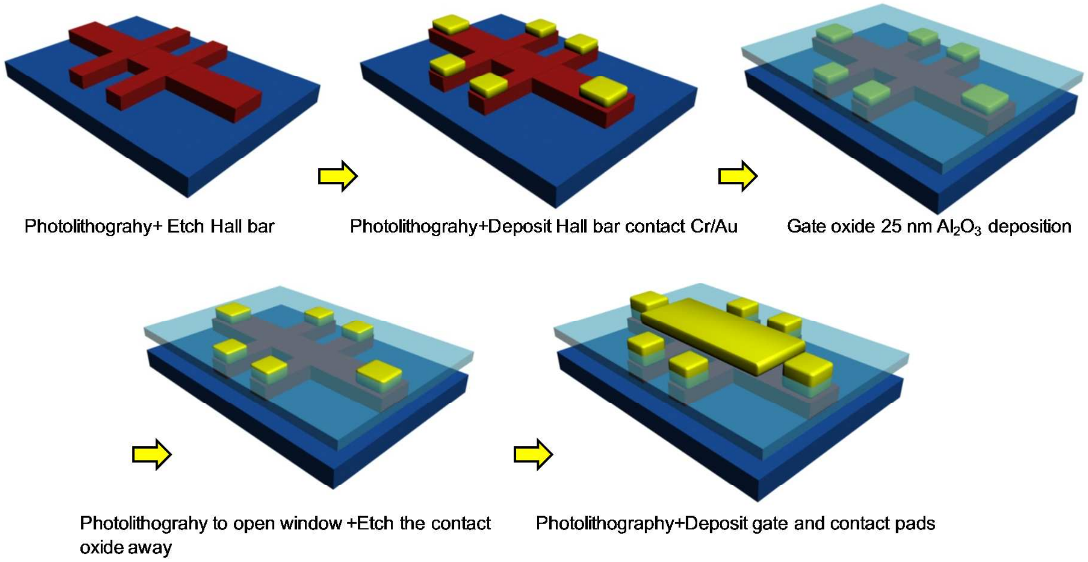

Photolithograhy+ Etch Hall bar

Photolithograhy+Deposit Hall bar contact Cr/Au

Gate oxide 25 nm Al_2O_3 deposition

Photolithograhy to open window +Etch the contact oxide away

Photolithography+Deposit gate and contact pads

Figure S2. Fabrication processes of TI based FET by photolithography.

4. Maximum Resistance and 2D Carrier Density vs. Thickness

The thickness dependent maximum resistant R_{max} obtained from Figure 2 in the main text, presents an abrupt change at 4 QL, as indicated in Figure S3. At 4 QL, $R_{\max}$ reaches ~ 70 kΩ, owing to the surface bandgap opening (~180 meV) at the Dirac point. As film thickness increases, $R_{\max}$ decreases monotonically as the surface gap vanishing and continuously increased bulk contribution.

At the same time, the 2D carrier concentration n_H remains low value < 2.5×10^{12} cm^{-2} for thickness below 8 QL, where bulk contribution is greatly suppressed. However, it is noted that the n_H suddenly jumps to 7.5×10^{12} cm^{-2} at $t \geq 8$ QL, above which gate may not effectively modulate the charge carrier density of the entire film any more. Hence, in order to suppress bulk contribution and achieve low density TI sample, film thickness should be kept below ~8 QL. This is consistent with the literature that by solving Poisson equation, the first order estimated maximum depletion width D is ~ 11 nm, beyond which a portion of carriers cannot be fully depleted by gating effect.[5]

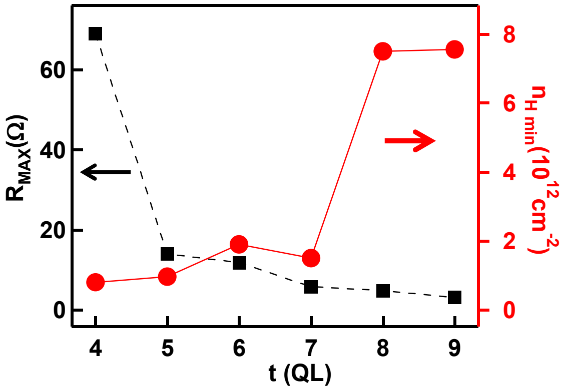

Figure S3. $R_{\max}$ and n_H as functions of thickness. The largest $R_{\max}$ is obtained at 4 QL and it rapidly decreases as thickness increases. n_H remains < 2.5×10^{12} cm^{-2} for 4 to 7 QLs, and suddenly increases to 7.5×10^{12} cm^{-2} at $t \geq 8$ QL.

5. Quantum interferences competition in 5 QL sample.

For completeness, we also verify the WAL/WL quantum interference modes in the 5 QL film at 0.3 K as shown in Figure S4**a**. The inset of Figure S4**b** presents the gate voltage dependence of resistance, in which we roughly define the ambipolar region (-12 V < V_g < 4 V) and n-type region ($V_g \geq 4$ V). In Figure S4**a**, in the ambipolar region, the MC curves firstly display WL-like behavior at low field, and then bend over to WAL at higher field, similarly as

4 QL case. The WAL characteristics prevail at the unipolar region, possibly because now E_F moves into the upper surface state branch. The evolution of both α_0 (upper panel) and α_1 (lower panel) fitted by Eq. 2 as functions of gate voltage is present in Figure S4**b**. The WAL contribution $|\alpha_0|$ enhances when V_g moves from the ambipolar to the unipolar region, whereas the $|\alpha_1|$ representing WL contribution monotonically decreases.

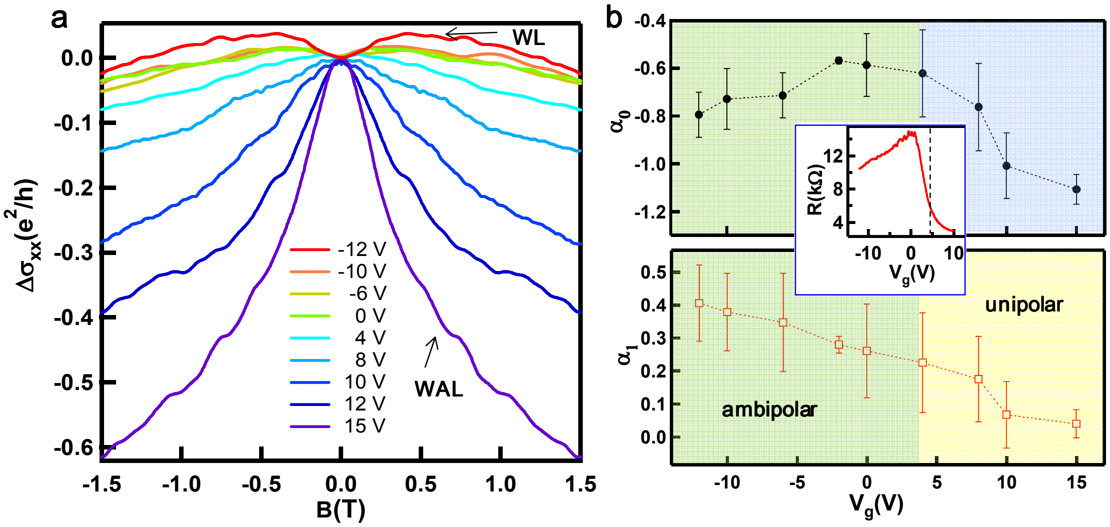

Figure S4. Quantum interference competition in 5 QL $(Bi_{0.57}Sb_{0.43})_2Te_3$ at 0.3 K. a, Evolution of normalized low field MC as a function of gate voltage. In the ambipolar region (-12 V < V_g < 4 V), where E_F is close to the surface band gap, the MC curves firstly show WL-like behavior at low magnetic field, and then bend over to WAL at higher field. The WAL characteristics prevail in the unipolar region ($V_g \geq$ 4 V) when E_F moves into the upper surface state branch. **b**, The evolution of α_0 (upper panel) and α_1 (lower panel) fitted by Eq. 2 as functions of gate voltage. The WAL contribution $|\alpha_0|$ enhances when V_g moves from the ambipolar into the unipolar region, whereas WL contribution $|\alpha_1|$ decreases. Inset: gate voltage dependence of resistance for the 5 QL sample.

6. Weak antilocalization in 6 ~10 QLs.

Figure S5 **a-d** demonstrate detailed gated voltage dependence of the normalized magnetoconductivity (MC) $\Delta\sigma(B) = \sigma_{xx}(B) - \sigma_{xx}(0)$ of 6, 7, 9, 10 QLs films at T = 0.3 K. All samples present clear weak antilocalization signature, in which $\Delta\sigma(B)$ has a cusp-like maximum at $B = 0$. The 6 QL sample shows more dramatic gate dependence of $\Delta\sigma(B)$ than thicker ones owing to its lower carrier density.[6] One component Hikami-Larkin-Nagaoka theory (Eq. 1 in the main text) is applied to fit the prefactor α and phase coherent length l_ϕ. $|\alpha|$ in Figure S5 **e-h** show their maxima ($|\alpha|$~1) as E_F is tuned close to the Dirac point, implying the topological properties is clearly revealed at charge neutrality point. As E_F moves far away, it corresponds to the case of coherently coupled bulk and surface electron states since more bulk carriers are accumulated, hence $|\alpha|$ and l_ϕ reduces. Furthermore, as film thickness increases, the gate-dependent $|\alpha|$ increases from 0.57~1.04 for 6 QL to 1.01~1.19 for 10 QL, suggesting increased channel separation with thickness.

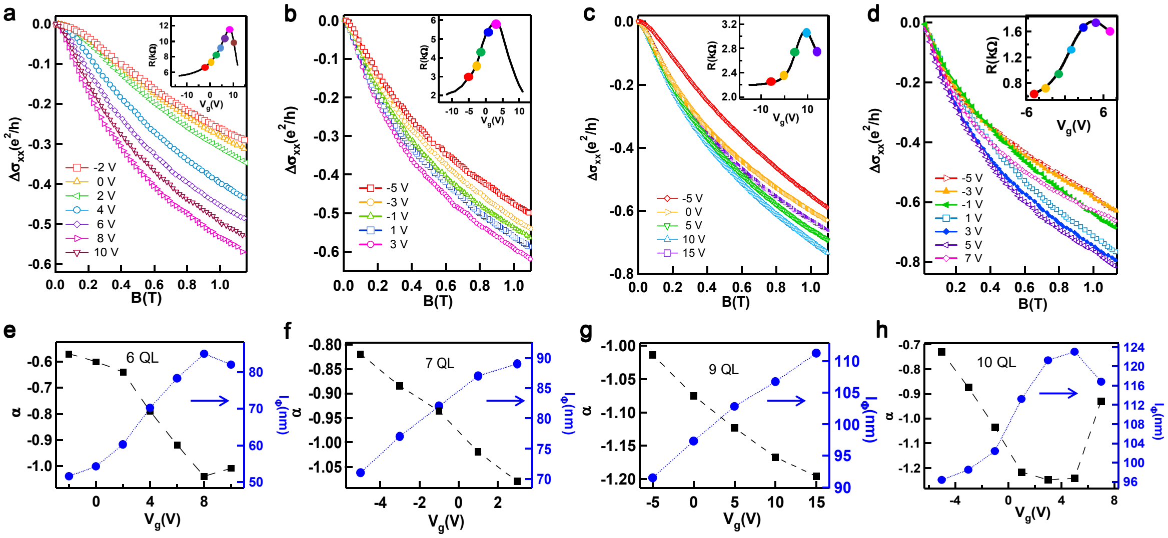

Figure S5. Gate voltage dependence of α and l_ϕ in 6, 7, 9, 10 QLs samples at 0.3 K. a-d, The gate voltage dependence of normalized magnetoconductance of 6 QL(**a**), 7 QL(**b**), 9 QL(**c**), 10 QL (**b**). Inset: The gate voltage dependence of resistance for the corresponding thin film, where the solid circles present the corresponding gate voltages applied. **e-h,** Fitted phase coherence length l_ϕ (squares) and coefficient α (circles) from one component HLN theory (Eq. (1)) as functions of gate voltage for 6 QL(**a**), 7 QL(**b**), 9 QL(**c**), 10 QL(**b**).

7. Theoretical calculation of two parameters α_0 and α_1.

In the two-component HLN thoery, the two parameters α_0 and α_1 present the weight of WAL and WL, respectively, and both of which depend on the position of E_F respective to the surface Dirac point. According to the Ref. 7-8, α_0 and α_1 are derived as following forms. Here we obtained these simplified formula by assuming that the magnetic scattering length $l_m \to \infty$, since magnetic impurity is absent in our samples.

$$\alpha_0 = -\frac{a^4 b^4}{(a^4+b^4)(a^4+b^4-a^2b^2)} \quad \alpha_1 = \frac{(a^4+b^4)(a^2-b^2)^2}{2(a^4+b^4-a^2b^2)^2}$$

where $a \equiv \cos\frac{\Theta}{2}$, $b \equiv \sin\frac{\Theta}{2}$. Here, Θ is defined as $\cos\Theta = \frac{\Delta/2 - Bk_F^2}{E_F - Dk_F^2}$, where Δ is the surface band gap. *B* and *D* are the parameters in the model Hamiltonian in Ref. 7 , in which B represents the 2nd order correction to the gap size at non-zero momentum and D corresponds to the bulk kinetic energy dispersion coefficient, respectively. At the Dirac point, the relation can be simplified as $\cos\Theta \approx \frac{\Delta/2}{E_F}$. The corresponding Berry phase as shown in Ref. 7 is given by $\phi = \pi(1-\cos(\Theta))$.

As discussed in Ref. 8, the quantum interference behavior (WAL/WL) is mainly controlled by $\cos\Theta$. In the limit when E_F is far into the upper surface state (conduction) branch or the lower (valence) branch, *i.e.*, $\cos\Theta \to 0$, corresponding to $\alpha_0 = -1/2$, $\alpha_1 = 0$, one has only WAL with negative MC cusp. However, as E_F is moved toward the surface gap controlled by applying the gate voltage, $\cos\Theta$ increases and consequently drive the system first into the unitary regime; and eventually reach the WL regime with positive MC cusp when $\cos\Theta \to 1$ ($\alpha_0 = 0$, $\alpha_1 = 1/2$).

REFERENCE

1. Taskin, A. A.; Sasaki, S.; Segawa, K.; Ando, Y. *Physical Review Letters* **2012,** 109, (6), 066803.
2. He, L.; Xiu, F.; Wang, Y.; Fedorov, A. V.; Huang, G.; Kou, X.; Lang, M.; Beyermann, W. P.; Zou, J.; Wang, K. L. *Journal of Applied Physics* **2011,** 109, (10), 103702.
3. Liu, M.; Chang, C.-Z.; Zhang, Z.; Zhang, Y.; Ruan, W.; He, K.; Wang, L.-l.; Chen, X.; Jia, J.-F.; Zhang, S.-C.; Xue, Q.-K.; Ma, X.; Wang, Y. *Physical Review B* **2011,** 83, (16), 165440.
4. Lang, M.; He, L.; Xiu, F.; Yu, X.; Tang, J.; Wang, Y.; Kou, X.; Jiang, W.; Fedorov, A. V.; Wang, K. L. *ACS Nano* **2011,** 6, (1), 295-302.

5. Kong, D.; Chen, Y.; Cha, J. J.; Zhang, Q.; Analytis, J. G.; Lai, K.; Liu, Z.; Hong, S. S.; Koski, K. J.; Mo, S.-K.; Hussain, Z.; Fisher, I. R.; Shen, Z.-X.; Cui, Y. *Nat Nano* **2011,** 6, (11), 705-709.
6. Chen, J.; Qin, H. J.; Yang, F.; Liu, J.; Guan, T.; Qu, F. M.; Zhang, G. H.; Shi, J. R.; Xie, X. C.; Yang, C. L.; Wu, K. H.; Li, Y. Q.; Lu, L. *Physical Review Letters* **2010,** 105, (17), 176602.
7. Lu, H.-Z.; Shen, S.-Q. *Physical Review B* **2011,** 84, (12), 125138.
8. Lu, H.-Z.; Shi, J.; Shen, S.-Q. *Physical Review Letters* **2011,** 107, (7), 076801.